Journal of Clinical and Nursing Research, 2024, Volume 8, Issue 12
http://ojs.bbwpublisher.com/index.php/JCNR
Online ISSN: 2208-3693
Print ISSN: 2208-3685

Near-Infrared Light-Responsive Cubic Vesicles for Enhanced Blood-Brain Barrier Permeability and Drug Delivery

Xinyu Wang[1,2], Xiaorong Zheng[3,4], Junfei Li[3,4],Changming Shen[3,4], Hongyan Zhang[3,4], Jianwei Jiang[3,4]*

[1]Department of Pharmacy, Hangzhou TCM Hospital Affiliated to Zhejiang Chinese Medical University, Hangzhou 310007, Zhejiang Province, China
[2]Department of Pharmacy, Hangzhou Hospital of Traditional Chinese Medicine, Hangzhou 310007, Zhejiang Province, China
[3]Zhejiang Cancer Hospital, Hangzhou 310022, Zhejiang Province, China
[4]Hangzhou Institute of Medicine, Chinese Academy of Sciences, Hangzhou 310022, Zhejiang Province, China

***Corresponding author:** Jianwei Jiang, jiangjw@zjcc.org.cn

Abstract: Delivering therapeutic agents to the central nervous system (CNS) is challenging due to the blood-brain barrier (BBB). This study presents a novel approach utilizing near-infrared (NIR) light-responsive gold-coated cubic vesicles (Auslip) to modulate BBB permeability and enhance drug delivery to glioma cells. Upon NIR activation, Auslip releases encapsulated agents and transiently opens the BBB. The results demonstrate that Auslip increases doxorubicin (DOX) delivery to glioma C6 cells in a co-culture model with human brain microvascular endothelial cells (hCMEC/D3). This approach offers a promising strategy for CNS therapeutics by enabling simultaneous BBB opening and drug release through optical stimulation.

Keywords: Controlled drug release; Blood-brain barrier; Liposome; Gold nanoparticles; Drug delivery

Online publication: December 31, 2024

1. Introduction

The blood-brain barrier (BBB), primarily composed of brain capillary endothelial cells supported by pericytes and astrocytes, acts as a protective interface between the circulatory system and the brain [1,2]. While the BBB facilitates the exchange of essential nutrients, it prevents the passage of most hydrophilic and large molecules, posing a significant challenge for central nervous system (CNS) therapeutics [3,4]. Approximately 98% of small molecules are delivered systemically and nearly all large molecules are excluded by the BBB [5]. Currently, no safe and efficient method exists to overcome this barrier [6], underscoring the urgent need for strategies to enhance BBB

permeability [7,8].

Several approaches have been explored to temporarily disrupt the BBB. These include osmotic disruption with hypertonic mannitol [9], the use of vasoactive peptides to increase whole-brain permeability [10], and enhancing drug transport via cell-penetrating peptides or active targeting ligands [11]. Nanoparticle-based drug delivery systems have also been investigated as a means to facilitate drug passage across the BBB [12]. For example, polyethylene glycol-coated liposomes have demonstrated potential in improving brain drug delivery [13]. Focused ultrasound (FUS) excitation of circulating microbubbles is a well-established technique for increasing BBB permeability [14]; however, the risks associated with repeated FUS treatments remain a concern [15]. Additionally, receptor-mediated transcytosis targeting BBB transporters has shown promise but often suffers from limitations in specificity and efficiency [16].

Qin *et al.* reported that laser excitation of gold nanoparticles generates mechanical waves capable of temporarily increasing BBB permeability [17]. While this method offers high spatial control compared to other non-optical techniques, it has certain limitations: it relies on visible light (532 nm), which has poor tissue penetration (less than 2.5 mm) [18], and gold nanoparticles exhibit limited drug-loading capacity. In contrast, near-infrared (NIR) light provides deeper tissue penetration and reduced photodamage, making it more suitable for *in vivo* applications [19,20]. Liposome-based carriers, meanwhile, offer a versatile platform for drug encapsulation and controlled release [21].

This study proposes the use of NIR-responsive gold-coated vesicles (Auslip) to enhance drug transport across the BBB. NIR short-pulsed laser irradiation (750 nm; 28 ps) generates mechanical waves via surface plasmon resonance of the gold shell [22]. These waves transiently open the BBB and increase vesicle membrane permeability, resulting in the rapid release of encapsulated cargo and its subsequent transport across the BBB (**Figure 1A**). The use of NIR light allows deeper tissue penetration, while liposomes enable the encapsulation of various therapeutic agents. This strategy creates high local drug concentration gradients and facilitates simultaneous BBB opening.

This study demonstrates that Auslip exhibits a cubic morphology and responds effectively to NIR picosecond laser activation. NIR laser stimulation (20 mJ/cm², 28 ps) generates nanobubbles around Auslip, which collapse within 1 ms. The resulting mechanical waves release encapsulated fluorescent probes and transiently increase permeability in hCMEC/D3 monolayers. Enhanced doxorubicin delivery to glioma C6 cells was observed in a co-culture model with hCMEC/D3 cells. These findings suggest that Auslip represents a promising carrier for brain-targeted drug delivery.

2. Methodology

2.1. Materials

Distearoylphosphatidylcholine (DSPC), 1,2-dipalmitoyl-sn-glycero-3-phosphothioethanol (DPPTE), and cholesterol were purchased from Avanti Polar Lipids. Fluorescein isothiocyanate-labeled dextran (FITC-dextran, 40 kDa), anti-JAM-A antibody BV11, and Triton X-100 were obtained from MilliporeSigma. Ascorbic acid, borate buffer, Dulbecco's Modified Eagle Medium (DMEM), fetal bovine serum (FBS), 4',6-diamidino-2-phenylindole (DAPI), and doxorubicin hydrochloride were used as received.

2.2. Preparation of Auslip

Tight junction (TJ)-targeting gold-coated thiolate vesicles (Auslip) were prepared using a three-step method.

2.2.1. Preparation of thiolate liposomes (Slip)

Slip was prepared using the thin-film hydration method. DSPC, DPPTE, and cholesterol (molar ratio 6:3:1) were dissolved in chloroform, and the solvent was evaporated to form a thin lipid film. The film was hydrated with phosphate-buffered saline (PBS, pH 7.4) at 65°C for 30 minutes with gentle shaking. The resulting suspension was extruded through a 200 nm polycarbonate membrane to obtain uniform liposomes.

2.2.2. Preparation of gold-coated Slip

A previously reported *in situ* gold reduction method was employed to achieve gold coating [12]. Briefly, the Slip was diluted to 1 mM using HEPES buffer. A gold chloride solution (20 mM) was added and mixed with Slip, followed by the addition of an ascorbic acid solution (40 mM). After reduction, the gold-coated Slip was dialyzed against HEPES buffer for 24 hours at 4°C to remove unreacted gold chloride and ascorbic acid.

2.2.3. Preparation of TJ-targeting gold-coated thiolate vesicles (Auslip)

The anti-JAM-A antibody BV16 was conjugated to the surface of Slip via Au-S bonds. Thiols react directly with the oxidized gold surface to form Au-S bonds through an oxidation-reduction reaction. To prepare thiolated BV16, BV16 was reacted with orthopyridyl-disulfide-polyethylene glycol-N-hydroxysuccinimide ester (OPSS-PEG-NHS). OPSS-PEG-NHS in $NaHCO_3$ (10 mM, pH 8.5) was added to the BV16 solution at a 100:1 molar ratio. The mixture was vortexed, and dialysis was performed for 4 hours at 4°C to remove unreacted OPSS-PEG-NHS. Thiolated BV16 was subsequently reacted with Slip at a molar ratio of 100:1 for 1 hour on ice. The BV16-modified Slip (Auslip) was washed three times and stored at 4°C until use.

2.3. Characterization of Auslip

The hydrodynamic diameter and polydispersity of Auslip and Slip were measured using dynamic light scattering with a Zetasizer (Nano ZS; Malvern Panalytical). UV-vis spectra in the range of 400–1000 nm were recorded using a spectrometer. The morphology of Auslip was observed using transmission electron microscopy (TEM) operating at 200 kV. Auslip samples, diluted with PBS, were dropped onto carbon film-coated copper grids, air-dried for 30 minutes at room temperature, and imaged at 125K magnification.

2.4. Characterization of near-infrared light-triggered drug release

The release kinetics of Auslip were monitored through real-time imaging during NIR laser activation. Calcein-loaded Auslip was placed into a capillary sealed with mineral oil and immobilized on the stage of an inverted microscope (Olympus IX73). The picosecond laser beam was focused on a 400 μm diameter spot. Auslip was positioned at the center of the focused laser beam and stimulated with a single 28 ps laser pulse (20 mJ/cm², 750 nm). The fluorescence intensity of Auslip suspensions before and after laser irradiation was observed using an inverted fluorescence microscope.

To quantify calcein release, Auslip was placed in a black 384-well plate, and the laser beam size was adjusted to 4 mm to cover the entire well. Suspensions were exposed to the laser beam at varying laser energies (10, 20, 50, and 100 mJ/cm²). Fluorescence was measured immediately after laser treatment, and the release percentage was calculated using the following equation:

Release percentage (%)=$(F_x - F_0)/(F_t - F_0)$

where F_x is the fluorescence after laser irradiation, F_0 is the initial fluorescence, and F_t is the fluorescence

after 100% release induced by 1% Triton X-100 treatment.

The formation of plasmonic nanobubbles following NIR laser stimulation of Auslip was monitored using an optical pump-probe method. Nanobubbles generated by laser excitation scattered a continuous laser beam (probe at 690 nm), leading to a decrease in transmitted intensity. Axial intensity changes in the probe beam were recorded using a digital oscilloscope for time-response analysis [20].

2.5. Cell culture

Human brain microvascular endothelial (hCMEC/D3) cells were cultured in ECM supplemented with 10% FBS. C6 glioma cells were cultured in DMEM/F12 medium containing 10% FBS. All cells were incubated at 37°C.

An *in vitro* BBB model was established as previously reported with minor modifications [21]. hCMEC/D3 cells were seeded at a density of 5×10^5 cells/well in Transwell inserts (12 wells/plate, 0.3 cm², pore size 8 μm). ECM medium was added to the lower chamber, and transendothelial electrical resistance (TEER) values were measured using Millicell ERS. The monolayer was deemed established when TEER exceeded 70 Ω·cm².

For a co-culture model, collagen-coated coverslips were placed in the lower chamber, and C6 cells were seeded at a density of 1×10^5 cells/well. Transwell inserts with hCMEC/D3 cells meeting BBB model criteria were placed in the upper chamber.

2.6. Characterization of optical-triggered blood-brain barrier opening in hCMEC/D3 cell model

The culture medium in the cellular monolayers was replaced with a medium without 5% FBS, and the system was transferred to 96-well black plates. A total of 100 μL of culture medium was replaced in the bottom chamber to maintain a constant volume. The fluorescence intensity of collected samples was measured at an excitation wavelength of 490 nm and an emission wavelength of 540 nm to determine the FITC-dextran concentration. The quantity (Q) was calculated by multiplying the concentration by the volume. The apparent permeability (P_{app}, cm/s) was calculated as:

$$P_{app} = \frac{dQ}{dT \times A \times C}$$

where dQ/dT is the rate of FITC-dextran quantity change over time, A is the membrane surface area, and C is the initial dextran concentration.

For *in vitro* transient BBB opening, hCMEC/D3 monolayers were seeded on Transwell inserts for approximately one week, forming a barrier with a TEER value of ~70 Ω·cm² and a P_{app} value of $8.4 \pm 1.4\times10^{-7}$ cm/s for 40 kDa FITC-dextran. The cellular monolayers were incubated with Auslip for 30 minutes at 37°C in a 5% CO_2 environment. Following incubation, the monolayers were stimulated with a 28 ps laser (20 mJ/cm², 750 nm). The BBB opening was assessed by monitoring changes in TEER values and FITC-dextran permeability. Immunostaining of the tight junction protein ZO-1 was also performed before and after NIR laser stimulation to evaluate structural changes.

2.7. Measurement of enhanced doxorubicin delivery in in vitro glioma model

To assess enhanced doxorubicin delivery, a similar BBB-opening procedure was performed using the hCMEC/D3 and C6 glioma cell co-culture model. Doxorubicin-loaded Auslip was incubated with hCMEC/D3 monolayers for

30 minutes at 37°C in a 5% CO_2 environment. The monolayers were then stimulated using a 28 ps laser (20 mJ/cm², 750 nm) and further incubated for 30 minutes under the same conditions.

Following the treatment, C6 glioma cells in the lower chamber were fixed and stained with DAPI. Fluorescence imaging was conducted using a confocal microscope to assess doxorubicin accumulation in the glioma cells.

3. Results and discussion

3.1. Characterization of Auslip

The hydrodynamic size of the naked Slip was approximately 100.7 nm, which increased to 126.6 nm after gold coating and antibody conjugation (**Table 1**). Doxorubicin (DOX)-loaded Auslip exhibited a size of 131.2 nm. All vesicles demonstrated low polydispersity indices (< 0.2), indicating high uniformity.

Transmission electron microscopy images revealed that Auslip exhibited an unexpected cubic morphology with a continuous gold shell (**Figure 1B**). UV-vis spectra showed a prominent absorption peak at approximately 750 nm (**Figure 1C**), suggesting suitability for near-infrared (NIR) activation. The term "Slip" refers to thiolated liposomes prepared with DPPTE, which provides thiol groups for subsequent gold coating. Vesicles generally consist of lipid bilayers designed for drug encapsulation. Following gold coating, Slip transformed into Auslip.

Table 1. Hydrodynamic diameter and polydispersity of uncoated thiolate vesicle (Slip), blank TJ-targeting gold coated vesicles (Auslip), and calcein or doxorubicin encapsulated Auslip

	Size (nm)	PDI
Slip	100.7 ± 9.9	0.113 ± 0.083
Auslip	126.6 ± 7.1	0.141 ± 0.040
Calcein loaded Auslip	139.0 ± 9.7	0.175 ± 0.062
Doxorubicin loaded Auslip	131.2 ± 15.5	0.117± 0.060

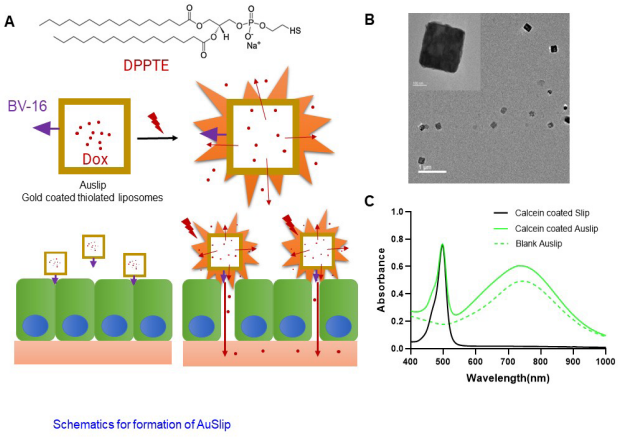

Figure 1. Cubic light-responsive vesicles for blood-brain barrier opening and burst drug release. **(A)** Schematic representation of the formation of cubic light-responsive vesicles (Auslip). **(B)** Representative TEM images of cubic Auslip. **(C)** UV-vis spectra of cubic Auslip, gold-coated tight junction (TJ)-targeting thiolated vesicles (Auslip), and Slip, which refers to thiolated liposomes without gold coating on the surface

3.2. Near-infrared laser-triggered release

To evaluate NIR picosecond (ps) pulsed laser-activated drug release, a self-quenching fluorescent dye, calcein disodium, was encapsulated within Auslip. At high concentrations, calcein fluorescence is quenched due to self-association effects. Upon release from Auslip and dilution by the surrounding buffer, calcein fluorescence de-quenches, leading to an increase in fluorescence intensity. Auslip samples were loaded into a capillary with an inner diameter of approximately 400 µm and activated using a ps NIR laser.

Live fluorescence imaging demonstrated an immediate increase in fluorescence intensity in the irradiated region following light activation (750 nm, 28 ps, single pulse) (**Figure 2A**). Fluorescence analysis revealed that light activation triggered a rapid release of calcein, with the maximum release observed within 0.5 ms.

To understand this rapid release pattern, nanobubble generation induced by NIR irradiation of Auslip was investigated using an optical pump-probe technique. At a laser intensity of 10 mJ/cm², nanobubble generation was not detected. However, increasing the intensity to 20 mJ/cm² resulted in the formation of nanobubbles, which expanded and collapsed within 750 ns (**Figure 2C**). In contrast, nanobubbles were not observed for Slip, indicating the absence of calcein release upon NIR irradiation in the absence of a gold coating. The short lifetime of the nanobubbles likely explains the rapid release of calcein from Auslip upon optical activation.

Quantitative measurements demonstrated that laser intensity modulated the extent of calcein release. A single laser pulse with an intensity of 20 mJ/cm² triggered the release of over 75% of encapsulated calcein, while increasing the intensity to 100 mJ/cm² further enhanced the release to 93%. To minimize potential cell damage, Auslip activation was performed at a laser intensity of 20 mJ/cm² (**Figure 2D**). Notably, ps NIR irradiation failed to induce calcein release from Slip, further confirming that the surface gold coating is essential for opto-triggered release.

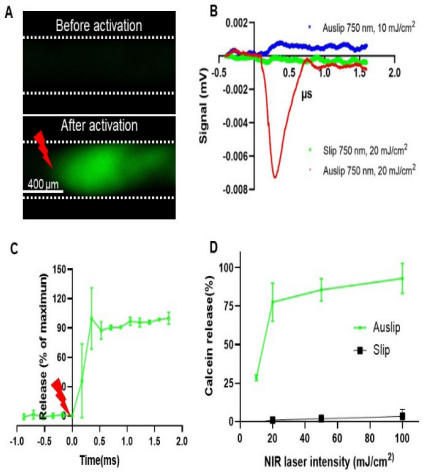

Figure 2. Near-infrared pulsed laser activation triggered calcein release from Auslip. **(A)** Representative fluorescence images of Auslip-filled capillaries before and after light activation. **(B)** Measurement of nanobubbles generated upon NIR light activation. **(C)** Kinetics of calcein release following NIR light activation (750 nm, 20 mJ/cm², single pulse). **(D)** Quantitative analysis of calcein release from Auslip and Slip upon activation by a single pulse with laser intensities ranging from 10 to 100 mJ/cm²

3.3. Characterization of optical-triggered blood-brain barrier opening in hCMEC/D3 cell model

Transendothelial electrical resistance, transport of fluorescein isothiocyanate-dextran 40 kDa (FD40) across the monolayer, and immunofluorescence staining of ZO-1 were monitored to evaluate light-stimulation-triggered BBB opening in the hCMEC/D3 cell monolayer. The results demonstrated that a single 750 nm picosecond (ps) laser pulse activation caused an immediate decrease in TEER for hCMEC/D3 monolayers pre-treated with Auslip. The TEER reached its minimum value, approximately 45%, at 30 minutes post-light stimulation (**Figure 3A**). In contrast, no significant changes were observed in hCMEC/D3 monolayers treated with Slip under light stimulation or Auslip without light activation throughout the experimental time course. TEER gradually recovered to pre-stimulation levels within 3 hours.

A transport study of FD40 conducted immediately after light stimulation indicated that the apparent permeability (P_{app}) of FD40 increased from 8.4×10^{-7} cm/s to 3.4×10^{-6} cm/s in hCMEC/D3 monolayers treated with Auslip and NIR activation (**Figure 3B**). By comparison, FD40 transport profiles remained unchanged in hCMEC/D3 monolayers treated with Slip and NIR activation or Auslip without light stimulation. These results confirmed that both Auslip treatment and NIR light activation were required for BBB opening.

Immunofluorescence staining of ZO-1 protein further supported the findings, revealing disrupted tight junctions (TJs) in the Auslip-treated hCMEC/D3 monolayer following NIR light activation (**Figure 3C**).

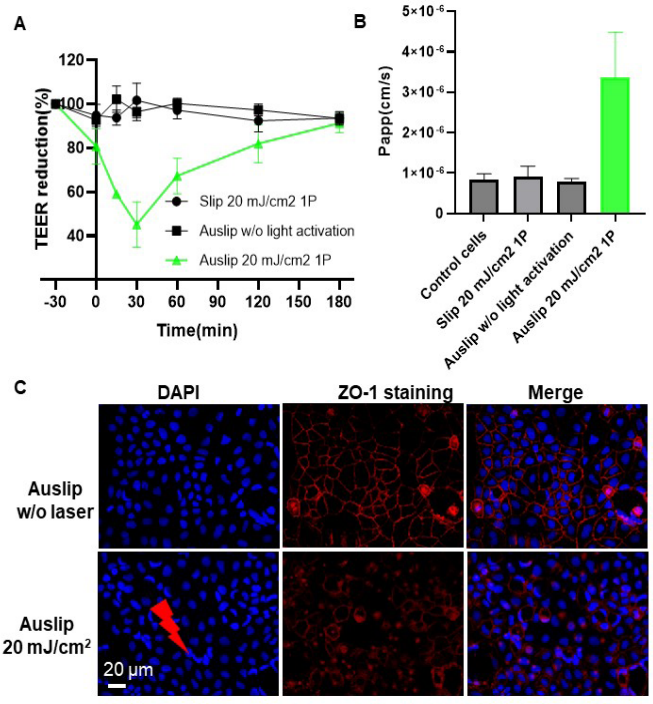

Figure 3. Near-infrared light-triggered blood-brain barrier opening in the hCMEC/D3 Cell model. **(A)** Transendothelial electrical resistance of the hCMEC/D3 cell monolayer treated with Slip or Auslip following NIR light activation. **(B)** Apparent permeability of FD40 across the hCMEC/D3 cell monolayer under various treatment conditions. **(C)** Immunofluorescence staining of ZO-1 protein in the hCMEC/D3 cell monolayer, showing tight junction integrity upon treatment with Auslip and NIR activation

3.4. Enhanced doxorubicin delivery in the C6 and hCMEC/D3 co-cultured cell model

Building on the increased permeability observed in the hCMEC/D3 cell monolayer, the potential of Auslip to enhance doxorubicin delivery through combined BBB opening and optically triggered burst release was investigated. The results demonstrated weak fluorescence in C6 cells co-cultured with hCMEC/D3 monolayers treated with NIR-activated Slip or Auslip without light activation (**Figure 4**). However, strong fluorescence was observed in C6 cells co-cultured with hCMEC/D3 monolayers treated with NIR-activated Auslip, with doxorubicin distributed throughout the cells. Quantitative fluorescence analysis showed that the fluorescence intensity in the NIR-activated Auslip group was 6.3 times higher than that of the NIR-activated Slip group.

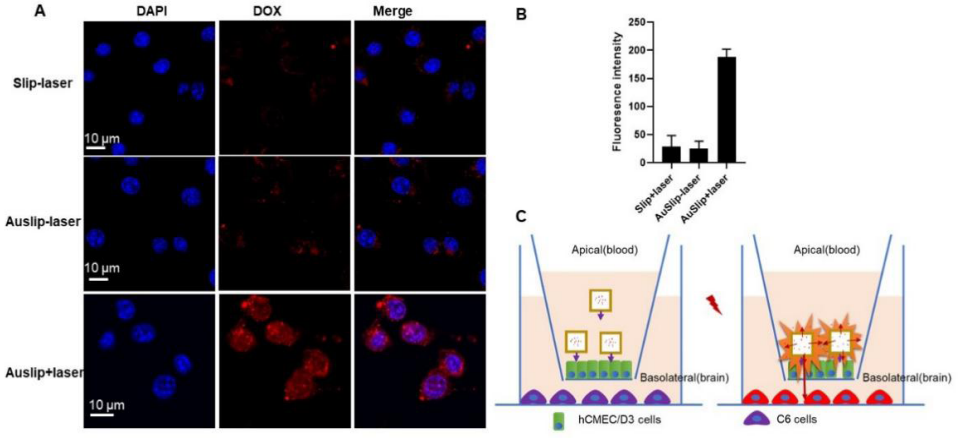

Figure 4. Enhanced doxorubicin delivery to glioma C6 cells in the hCMEC/D3 and C6 co-cultured cell model. **(A)** Representative fluorescence images of C6 cells treated with thiolated vesicles (Slip) or tight junction-targeting gold-coated thiolated liposomes (Auslip) in the presence or absence of NIR light activation (750 nm, 20 mJ/cm², single pulse). **(B)** Semi-quantitative analysis of fluorescence intensity in C6 cells treated with Auslip and Slip using ImageJ software. **(C)** Schematic illustration of enhanced doxorubicin delivery to glioma C6 cells. NIR activation triggered burst release of doxorubicin and transient loosening of tight junctions, facilitating doxorubicin transport across the hCMEC/D3 cell monolayer (apical side) and subsequent entry into C6 cells located in the basolateral chamber.

These results confirmed the enhanced drug delivery achieved through optically controlled BBB opening and burst release. The findings also highlighted the essential roles of both the gold coating on thiolated vesicles and NIR activation in facilitating this enhancement.

The BBB serves as a formidable barrier to brain drug delivery, excluding over 98% of therapeutic agents from entering the brain [22]. To address this challenge, a novel cubic tight-junction-targeting vesicle, Auslip, was developed. This system utilizes a NIR pulsed laser to transiently loosen tight junctions and trigger burst release of encapsulated cargos, thereby enhancing drug transport across the BBB. Both optically triggered BBB opening [10] and burst drug release [12,23] have been reported individually in recent years. However, this study represents the first instance in which the combination of these two techniques has been tested for enhanced drug delivery.

It was hypothesized that mechanical waves generated upon nanobubble collapse immediately disrupt the phospholipid bilayer of the vesicle, liberating encapsulated cargos and creating a high local drug gradient. The resulting mechanical phenomenon also transiently loosens tight junctions in the endothelial cell monolayer, thereby facilitating enhanced drug transport. This study demonstrated that stimulation of Auslip using a single 750

nm NIR laser pulse at an intensity of 20 mJ/cm² led to over 75% calcein release. Additionally, NIR stimulation immediately reduced TEER to 45% within 30 minutes, increased FD40 transport, and disrupted tight junctions in hCMEC/D3 cell monolayers pre-treated with Auslip. When combined, optical burst drug release and transient tight junction disruption increased doxorubicin transport into glioma C6 cells by more than six-fold.

The high photosensitivity observed in Auslip is likely attributable to its unique cubic morphology. Previous studies have demonstrated that faceted liposomes with stiff bilayers in the gel phase are susceptible to shear stress-induced disruption. Auslip exhibited a similar multi-faceted morphology, comparable to stress-sensitive liposomes. It is speculated that mechanical waves disrupt packing defects, compromising the integrity of Auslip, which is already under internal stress. Interestingly, the cubic structure was not intentionally designed but discovered unexpectedly. The gold coating method, which involves the in-situ reduction of gold chloride by ascorbic acid, typically results in spherical liposomes coated with small gold nanoparticles [12,17]. However, Auslip exhibited a continuous gold coating layer, leading to its cubic morphology. This transformation may be attributed to the presence of thiol groups on the liposome surface. Thiolated liposomes were selected to enhance gold coating through the formation of Au-thiol bonds. These bonds likely reinforce the gold-vesicle interaction, reorganizing the phospholipid bilayers into a multi-faceted structure. Further studies are necessary to elucidate the underlying molecular mechanisms.

One limitation of this study is the absence of *in vivo* proof-of-concept demonstrations. Tissue penetration of the light trigger remains critical for the application of optical BBB opening techniques. The absorbance spectrum of Auslip, which shows strong absorption of NIR light in the 650–850 nm range, suggests its potential for *in vivo* applications, as NIR light offers deeper tissue penetration into the brain. While Auslip has demonstrated promising results *in vitro*, further studies are required to evaluate its performance *in vivo*. Future investigations will focus on therapeutic agent delivery for disease treatment, the underlying mechanisms of action, and the effects on brain tissue.

4. Conclusion

This study presented novel cubic NIR light-responsive vesicles capable of enabling optically controlled BBB opening and burst drug release. Upon stimulation with a NIR picosecond laser pulse, Auslip generated mechanical waves that immediately liberated encapsulated cargo within 0.5 ms and transiently increased the permeability of the hCMEC/D3 monolayer by approximately four-fold. The combination of optically triggered BBB opening and burst drug release enhanced doxorubicin delivery to glioma C6 cells by 6.3-fold in an hCMEC/D3 and glioma C6 co-culture cell model. These findings demonstrate that Auslip represents a promising carrier for transient BBB opening and improved drug delivery to the brain. This approach, which enables simultaneous BBB opening and burst drug release upon optical stimulation, holds potential for the development of novel nanotherapeutics for CNS diseases.

Funding

The authors would like to acknowledge the Zhejiang Provincial Natural Science Foundation of China for supporting this project. This work was funded by the Joint Funds of the Zhejiang Provincial Natural Science Foundation of China, awarded to Jianwei Jiang (No. LBQ20H300001).

Disclosure statement

The authors declare no conflict of interest.

References

[1] Ding S, Khan AI, Cai X, et al., 2020, Overcoming blood-brain barrier transport: Advances in nanoparticle-based drug delivery strategies. Mater Today (Kidlington), 37: 112–125. https://doi.org/10.1016/j.mattod.2020.02.001

[2] Pardridge WM, 2005, The blood-brain barrier: bottleneck in brain drug development. NeuroRx, 2(1): 3–14. https://doi.org/10.1602/neurorx.2.1.3

[3] Chen ZA, Wu CH, Wu SH, et al., 2024, Receptor ligand-free mesoporous silica nanoparticles: a streamlined strategy for targeted drug delivery across the blood-brain barrier. ACS Nano, 12716–12736. https://doi.org/10.1021/acsnano.3c08993

[4] Zhao C, Zhu X, Tan J, et al., 2024, Lipid-based nanoparticles to address the limitations of GBM therapy by overcoming the blood-brain barrier, targeting glioblastoma stem cells, and counteracting the immunosuppressive tumor microenvironment. Biomed Pharmacother, 171: 116113. https://doi.org/10.1016/j.biopha.2023.116113

[5] Rapoport SI, 2000, Osmotic Opening of the Blood-Brain Barrier: Principles, Mechanism, and Therapeutic Applications. Cell Mol Neurobiol, 20(2): 217–230. https://doi.org/10.1023/a:1007049806660

[6] Smith-Cohn MA, Burley NB, Grossman SA, 2022, Transient Opening of the Blood-Brain Barrier by Vasoactive Peptides to Increase CNS Drug Delivery: Reality Versus Wishful Thinking? Curr Neuropharmacol, 20(7): 1383–1399. https://doi.org/10.2174/1570159X20999220131163504

[7] Li T, Bourgeois J-P, Celli S, et al., 2012, Cell-Penetrating Anti-GFAP VHH and Corresponding Fluorescent Fusion Protein VHH-GFP Spontaneously Cross the Blood-Brain Barrier and Specifically Recognize Astrocytes: Application to Brain Imaging. The FASEB Journal, 26(10): 3969–3979. https://doi.org/10.1096/fj.11-201384

[8] Fan CH, Ting CY, Chang YC, et al., 2015, Drug-Loaded Bubbles with Matched Focused Ultrasound Excitation for Concurrent Blood-Brain Barrier Opening and Brain-Tumor Drug Delivery. Acta Biomater, 15: 89–101. https://doi.org/10.1016/j.actbio.2014.12.026

[9] McMahon D, Poon C, Hynynen K, 2019, Evaluating the Safety Profile of Focused Ultrasound and Microbubble-Mediated Treatments to Increase Blood-Brain Barrier Permeability. Expert Opin Drug Deliv, 16(2): 129–142. https://doi.org/10.1080/17425247.2019.1567490

[10] Li X, Vemireddy V, Cai Q, et al., 2021, Reversibly Modulating the Blood-Brain Barrier by Laser Stimulation of Molecular-Targeted Nanoparticles. Nano Lett, 21(22): 9805–9815. https://doi.org/10.1021/acs.nanolett.1c02996

[11] Ash C, Dubec M, Donne K, et al., 2017, Effect of Wavelength and Beam Width on Penetration in Light-Tissue Interaction Using Computational Methods. Lasers Med Sci, 32(8): 1909–1918. https://doi.org/10.1007/s10103-017-2317-4

[12] Li X, Che Z, Mazhar K, et al., 2017, Ultrafast Near-Infrared Light-Triggered Intracellular Uncaging to Probe Cell Signaling. Adv Funct Mater, 27(11): 1605778. https://doi.org/10.1002/adfm.201605778

[13] Wang C, Xie Y, Song X, 2023, A NIR Programmable *In Vivo* miRNA Magnifier for NIR-II Imaging of Early Stage Cancer. Angew Chem Int Ed Engl, 62(50): e202312665. https://doi.org/10.1002/anie.202312665

[14] Wu D, Chen Q, Chen X, et al., 2023, The Blood-Brain Barrier: Structure, Regulation, and Drug Delivery. Signal Transduct Target Ther, 8(1): 217. https://doi.org/10.1038/s41392-023-01481-w

[15] Li Y, He D, Tu J, et al., 2018, The Comparative Effect of Wrapping Solid Gold Nanoparticles and Hollow Gold

Nanoparticles with Doxorubicin-Loaded Thermosensitive Liposomes for Cancer Thermo-Chemotherapy. Nanoscale, 10(18): 8628–8641. https://doi.org/10.1039/C7NR09083H

[16] Neuhaus F, Mueller D, Tanasescu R, et al., 2017, Vesicle Origami: Cuboid Phospholipid Vesicles Formed by Template-Free Self-Assembly. Angew Chem Int Ed Engl, 56(23): 6515–6518. https://doi.org/10.1002/anie.201701634

[17] Anderson JM, Langone JJ, 1999, Issues and Perspectives on the Biocompatibility and Immunotoxicity Evaluation of Implanted Controlled Release Systems. J Control Release, 57(2): 107–113. https://doi.org/10.1016/s0168-3659(98)00178-3

[18] Tagami T, Kubota M, Ozeki T, 2015, Effective Remote Loading of Doxorubicin into DPPC/Poloxamer 188 Hybrid Liposome to Retain Thermosensitive Property and the Assessment of Carrier-Based Acute Cytotoxicity for Pulmonary Administration. J Pharm Sci, 104(11): 3824–3832. https://doi.org/10.1002/jps.24593

[19] Saxena VK, Deb R, Shrivastava S, et al., 2012, Functionalizing Gold Nanoparticles with Bluetongue Virus Multiple Peptide Antigens Utilizing Gold–Thiol Interaction: A Novel Approach to Develop Pen Side Test. Res Vet Sci, 93(3): 1531–1536. https://doi.org/10.1016/j.rvsc.2012.04.013

[20] Galanzha EI, Nedosekin DA, Sarimollaoglu M, et al., 2013, Photoacoustic and Photothermal Cytometry Using Photoswitchable Proteins and Nanoparticles with Ultrasharp Resonances. J Biophotonics, 8(1–2): 81–93. https://doi.org/10.1002/jbio.201300140. Erratum in J Biophotonics, 8(8): 687. https://doi.org/10.1002/jbio.201580140

[21] Qiao L, Qin Y, Wang Y, et al., 2020, A Brain Glioma Gene Delivery Strategy by Angiopep-2 and TAT-Modified Magnetic Lipid-Polymer Hybrid Nanoparticles. RSC Advances, 10(68): 41471–41481. https://doi.org/10.1039/D0RA07161G

[22] Weissleder R, 2001, A Clearer Vision for *In Vivo* Imaging. Nat Biotechnol, 19(4): 316–317. https://doi.org/10.1038/86684

[23] Cherkasov VR, Mochalova EN, Babenyshev AV, et al., 2020, Antibody-Directed Metal-Organic Framework Nanoparticles for Targeted Drug Delivery. Acta Biomater, 103: 223–236. https://doi.org/10.1016/j.actbio.2019.12.012